Analysis of Lifting Operation of a Monopile Considering Vessel Shielding Effects in Short-crested Waves

Lin Li[1], Zhen Gao[1,2,3], and Torgeir Moan[1,2,3]
[1]Centre for Ships and Ocean Structures (CeSOS), NTNU, Trondheim, Norway
[2]Centre for Autonomous Marine Operations and Systems (AMOS), NTNU, Trondheim, Norway
[3]Department of Marine Technology, NTNU, Trondheim, Norway

ABSTRACT

This paper addresses numerical simulations of the lifting operation of an offshore wind turbine monopile foundation considering both shielding effects from the vessel and the spreading of the waves. A numerical model of the coupled monopile-vessel system is established. The disturbed wave field near the vessel is investigated and observed to be affected by the diffraction and radiation of the vessel. The shielding effects of the vessel during the lifting operation are accounted for in this study by interpolating fluid kinematics between pre-defined wave points near the vessel using SIMO software and an external Dynamic Link Library (DLL). The effects of short-crested waves on the wave field and on responses of the system are investigated by implementing the directional spreading function in the wave spectrum. Based on the time-domain simulations, the critical responses of the lifting system in various conditions are studied. The results indicate that the effects of the wave spreading are considerable in both incident and disturbed waves. The shielding effects are less significant in short-crested waves than in long-crested waves.

KEY WORDS: Lifting operation; short-crested waves; shielding effect; monopile; time-domain simulation.

INTRODUCTION

Monopile (MP) substructures are the most commonly used foundations for offshore wind farms in water depths up to 40 meters. It has been estimated that more than 75% of all installations are founded on monopiles by the end of 2013 (EWEA, 2014). Monopiles can be transported to site by the installation vessel or a feeder vessel, they can be barged to the site or can be capped and wet towed (Kaiser and Snyder, 2013). An offshore crane is often employed to upend the monopile to a vertical position and lower it down through the wave zone to the seabed. During the lifting operation, the monopile and the installation vessel are coupled through the lift wire and a gripper device which limits the horizontal motions of the monopile during the lowering. The monopile is lowered at a position which is very close to the hull of the crane vessel, so the wave forces on the monopile are affected by the presence of the vessel. Furthermore, since the lifting operation is commonly performed at a relative low sea states, the waves may spread in different directions and affect the motions of the vessel as well as the wave forces on the monopile. Therefore, it is of great interest to evaluate the effects of the wave spreading as well as the shielding effects from the vessel on the behavior of the lifting system.

Studies have been performed to investigate the heavy lifting operations in the oil and gas industry considering shielding effects, such as the lifting of a heavy load from a transport barge using a large capacity semi-submersible crane vessel (Mukerji, 1988; van den Boom et al., 1990; Baar et al., 1992). The studies found that the hydrodynamic interaction had little effect on the responses of the crane tip, but affected the responses of the transport barge and thus greatly affected the lifting operations because of the small dimension of the barge compared with that of the crane vessel (Baar et al., 1992). The sheltering effects from columns and caissons of a gravity-based substructure (GBS) on the barge during a float-over installation were studied (Sun et al., 2012). It has been shown the motions of the barge and the contact forces between the barge the GBS can be amplified due to the hydrodynamic interactions. Therefore, the hydrodynamic interaction between two floaters close to each other should be taken into consideration when estimating responses.

The approach to consider the shielding effects in those studies were to calculate the coupled hydrodynamic coefficients in frequency-domain when all the bodies are at their mean positions. This implies that the motions of all bodies in the system must be very small. However, when considering a continuous lowering operation that the positions of the lifted objects change continuously with time, the above method is not applicable. The main difficulty associated with this process lies in the large motion that the load might experience in waves during being lowered. Bai et al. (2014) introduced a 3D fully non-linear potential flow model to simulate the wave interaction with fully submerged structures either fixed or subjected to constrained motions in time-domain. The scenario of a cylindrical payload hanging from a rigid cable and subjected to wave actions was studied. However, the approach is limited to regular waves up to now and the simulation efficiency is low. The further application on more complicated operations and in irregular waves with longer duration is questionable.

In the case of lifting a monopile using a floating vessel, due to the small dimension of the monopile compared with the vessel, the hydrodynamic effects of the monopile on the vessel are minor and can be ignored. Li et al. (2014) introduced a method to account for the shielding effects from the installation vessel on a monopile during the entire lowering process. The wave forces on the monopile were calculated using Morison's equation by interpolating the disturbed wave kinematics at pre-defined wave points at each time step. It was concluded that the responses of the monopile can be significantly reduced in short waves when considering shielding effects. The study also showed it is possible to minimize the responses by choose a proper vessel heading using the shielding effects. However, only long-crested waves were considered when evaluating the shielding effects.

In the real sea condition, short-crested waves are found providing better accuracy for the wind generated seas and appear to be three-dimensional and complex (Chakrabarti, 1987; Goda, 2010; Kumar et al., 1999). The directional spreading of wave energy may give rise to forces and motions, which are different from those corresponding to long-crested waves. A large number of studies have been performed in recent years focusing on the directional wave effects on the forces and responses of various offshore structures e.g., large surface piercing circular cylinders (Isaacson and Nwogu, 1987; Nwogu, 1989; Zhu and Satravaha, 1995; Tao et al., 2007), long pipelines (Battjes, 1982; Lambrakos, 1982) , TLP platforms (Teigen, 1983), box-shaped structures (Isaacson and Sinha, 1986; Nwogu, 1989), and multiple floating bodies (Inoue and Islam, 2000; Sannasiraj et al., 2001). These studies showed significant effects on the loads and responses due to the spreading of the waves. The general observations were that the directional spreading of wave leads to a reduction of the loads in the main wave direction while the loads in the direction normal to the main wave direction can be greatly amplified due to the lateral disturbance in short-crested waves. The reduction of the loads due to the wave spreading sometimes can bring saving in fabrication costs. However, the spreading may also lead to a significant increase of the estimated fatigue life of an offshore structure (Marshall, 1976). For lifting operations with multi-body coupled systems, very little work has been published with short-crested irregular waves. However, the industry has been aware of the importance of the short-crested waves for lifting operations using a floating crane by establishing relevant guidance.

DNV (2014) recommended to assess whether long crested or short crested sea is conservative for the analysis concerned. It is suggested to investigate the effect of short-crested sea when the vertical crane tip motion is dominated by the roll motion in head sea ±15 deg. For simplicity, long-crested waves with a heading angle of ±20 deg can be applied to account for the additional effect from short-crested sea. Nevertheless, the guidance is very general and can hardly be applied for different situations. Moreover, there is no guidance or published work regarding how to evaluate the effects of the short-crested waves when accounting the shielding effects from the installation vessel.

The focus of the paper is to study the influences of the directional waves and the shielding effects of the vessel on the responses of the monopile lifting system. Time-domain simulations are performed using multi-body code SIMO (MARINTEK, 2012) and an external Dynamic Link Library (DLL) that included the shielding effects from the installation vessel (Li et al., 2014). The results in short-crested waves are compared with those in long-crested wave fields with the same total energy. The simulation model and the methodology are presented first, followed by discussions of the results. Finally, conclusions and recommendations are given for lifting operations regarding shielding effects and the influences from short-crested waves.

DESCRIPTION OF THE LIFTING SYSTEMS

A floating installation vessel was chosen for the monopile installation. The main dimensions of the vessel are presented in Table 1. The lifting capacity and the positioning system of the floating vessel made it capable of performing the installation of monopiles in shallow-water sites. The monopile used in the model was a long slender hollow cylinder with main dimensions listed in Table 1. Fig. 1 shows a schematic layout of the arrangement of the operation. The system included two rigid bodies, i.e., the floating installation vessel and the monopile. The two bodies are coupled through the lift wire and the gripper device. The set-up of the lifting system refers to Li et al. (2014).

Table 1: Main parameters of the floating installation vessel and the monopile (Li et al., 2014)

Vessel			Monopile		
Length overall	[*m*]	183	Total mass	[*ton*]	500
Breadth	[*m*]	47	Length	[*m*]	60
Draught	[*m*]	12	Outer diameter	[*m*]	5.7
Displacement	[*ton*]	52000	Thickness	[*m*]	0.06
Lifting capacity	[*ton*]	5000	Draft	[*m*]	20

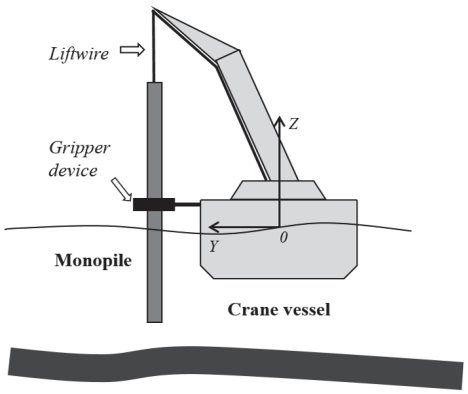

(a)

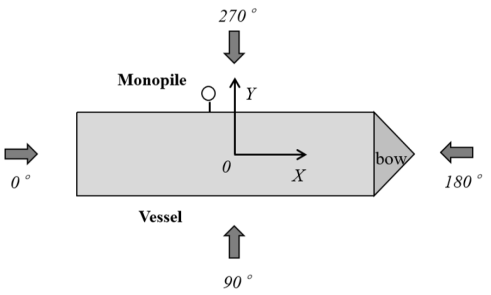

(b)

Figure 1: Monopile lifting arrangement (a) and definitions of global coordinate system (b)

The global coordinate system was a right-handed coordinate system with the following orientation: the X axis pointed towards the bow, the Y axis pointed towards the port side, and the Z axis pointed upwards. The origin was located at [mid-ship section, center line, still-water line] when the vessel was at rest. The crane tip position was chosen as [-20 *m*, 30 *m*, 80 *m*] in the global coordinate when the vessel was at rest. The water depth at the installation site was 25 meters, and the draft of the monopile in the time-domain simulations was constant 20 meters.

Table 2: Eigenperiods and eigenvectors of rigid body motions of coupled vessel-monopile lifting system (draft of MP = 20 *m*)

body	Mode		1	2	3	4	5	6	7	8	9	10	11
Vessel	Surge	[*m*]	0	0	-0.01	0	0.01	-0.03	-0.05	0	0	**0.89**	0
Vessel	Sway	[*m*]	0	-0.01	0	-0.01	0	0	-0.06	0.03	**0.91**	0	0.55
Vessel	Heave	[*m*]	0	0	0	0	0	-0.09	**0.99**	0	0.02	0	0.01
Vessel	Roll	[*deg*]	-0.03	0.01	0	-0.02	0	0	-0.12	**0.57**	0	0	-0.05
Vessel	Pitch	[*deg*]	0	0	0	0	-0.01	**0.3**	0.2	0	0	0	0.01
Vessel	Yaw	[*deg*]	0	0	0.01	0	-0.01	0	0	-0.01	**1**	0.02	**-0.76**
MP	Surge	[*m*]	0	0.02	**0.45**	-0.01	-0.05	-0.02	-0.06	0.01	**-0.63**	**1**	0.46
MP	Sway	[*m*]	0	**0.56**	-0.02	-0.03	0	0	-0.02	-0.12	**0.59**	-0.01	**1**
MP	Heave	[*m*]	**1**	0	0	-0.01	0	0.02	**1**	0.32	0.01	0	-0.02
MP	Roll	[*deg*]	0	**-1**	0.05	**1**	-0.02	-0.01	-0.29	**1**	0.05	0	0.1
MP	Pitch	[*deg*]	0	0.07	**1**	0.01	**1**	**1**	**0.63**	-0.01	0.08	-0.01	-0.04
Natura l period		[*sec*]	0.59	3.21	3.86	6.61	7.45	9.49	10.66	13.95	94.83	101.18	107.78

Two types of mechanical couplings between the vessel and the monopile were included in the numerical model: the wire coupling through the main lift wire and the coupling via the gripper device. The function of the gripper device was to control the horizontal motions of the monopile during lowering and landing as well as to support the monopile during driving operations. The gripper device was also rigidly fixed to the vessel. The detailed modelling of the mechanical couplings can refer to Li et al. (2014).

The equations of motion for the two-body coupled lifting system included 12 degrees of freedom (DOF s) and are given in Eqn. (1).

$$\left(\mathbf{M}+\mathbf{A}(\infty)\right)\cdot\ddot{\mathbf{x}}+\mathbf{D}_1\dot{\mathbf{x}}+\mathbf{D}_2 f\left(\dot{\mathbf{x}}\right)+\mathbf{K}\mathbf{x} + \int_0^t \mathbf{h}(t-\tau)\dot{\mathbf{x}}(\tau)d\tau=\mathbf{q}(t,\mathbf{x},\dot{\mathbf{x}}) \tag{1}$$

where,

M the total mass matrix;

x the rigid-body motion vector;

A the frequency-dependent added mass matrix ;

$\mathbf{D}_1$ the linear damping matrix;

$\mathbf{D}_2$ the quadratic damping matrix;

K the coupled hydrostatic stiffness matrix, including the hydrostatic stiffness of the vessel, the stiffness from the mooring line;

h the retardation function matrix of the vessel, which is calculated from the frequency-dependent added mass or potential damping using the panel method program WADAM (DNV, 2008);

q the external force vector. In the current model only the first order wave excitation forces forces $\mathbf{q}^{(1)}{}_{WA}$ are included for the floating vessel, and no second order wave forces were included. The wind and currents were also excluded for simplicity.

The external forces on the monopile included the gravity force, the buoyancy force, as well as the hydrodynamic wave forces. The wave forces normal to the MP's central axis were calculated by applying Morison's formula (Faltinsen, 1990). The monopile was divided into strips and the forces on the whole slender elements were calculated by strip theory. The wave forces $f_{W,s}$ per unit length on each strip of a moving circular cylinder normal to the member is as follows:

$$f_{W,s}=\rho_w C_M\frac{\pi D^2}{4}\cdot\ddot{\zeta}_s-\rho_w C_A\frac{\pi D^2}{4}\cdot\ddot{x}_s + \frac{1}{2}\rho_w C_q D\cdot|\dot{\zeta}_s-\dot{x}_s|\cdot(\dot{\zeta}_s-\dot{x}_s) \tag{2}$$

$\ddot{\zeta}_s$ and $\dot{\zeta}_s$ are fluid particle acceleration and velocity at the center of the strip, respectively; $\ddot{x}_s$ and $\dot{x}_s$ are the acceleration and velocity at the center of the strip due to the body motions; D is the outer diameter of the member; and C_M , C_A and C_q are the mass, added mass and quadratic drag force coefficients, respectively. The monopile was simulated as a slender body using strip theory, and the added mass and quadratic damping coefficients were selected according to Li et al. (2014).

The coupled eigenvectors and eigenvalues of the monopile-vessel lifting system are provided in Table 2, where the yaw motion of the monopile is excluded. The bold figures show the dominated rigid motions for each eigenvector. Modes 1-5 are dominated by monopile motions when the vessel is almost still. The vessel motions in heave, pitch and roll motions are coupled with the monopile motion and dominate modes 6-8. The other three modes are dominated by the vessel horizontal motions and corresponding to very long natural periods. It can be seen that the eigenvalues of modes 4 to 8 are in the range of 6 to 14 sec, which could be critical for the wave conditions concerned. The other modes are less critical for the responses during lifting. Moreover, in short waves with *Tp* less than 7.5 *sec* the resonant motions of the MP can be excited while in longer waves the contributions from the vessel motions may play an important role.

MODELLING OF THE SHIELDING EFFECTS

Due to the presence and the motions of the floating vessel in waves, the wave field near the vessel is different from the incident wave field. The hydrodynamic coefficients of the vessel and the fluid kinematics at any point in the wave field can be acquired in the frequency domain using potential theory. The wave fields including the effects of both radiation and diffraction of the vessel are defined as disturbed waves in this paper, which account for the vessel shielding effects. The undisturbed waves are defined as incident waves.

To calculate the wave forces on the monopile in the disturbed wave field, the fluid kinematics $\ddot{\zeta}_s$ and $\dot{\zeta}_s$ in Eqn. (2) should be consistent with the disturbed fluid kinematics. Because the position of the monopile changes in time, the fluid kinematics at each strip of the monopile are time- and position-dependent. Therefore, the approach proposed by Li et al. (2014) was applied to calculate the responses of the multi-body system in the time domain while considering the

shielding effects. However, the approach from Li et al. (2014) only considered long-crested waves and it is further developed in this paper to be able to include short-crested waves. The approach is briefly discussed here.

1. First, generate time series of disturbed fluid kinematics (fluid particle velocities and accelerations) at pre-defined wave points considering both shielding effects and wave spreading.

2. Then, at each time step of the simulation, determine the instantaneous position of each slender element based on the solutions from the previous time step. For each strip on the element, find the closest eight pre-defined wave points and apply a three-dimensional (3D) linear interpolation to obtain the fluid kinematics for this strip in disturbed waves.

3. Calculate the forces at each strip in disturbed waves using Eqn. (2) and then integrate along the submerged part of the slender element to acquire the total wave forces and moments on the structure.

4. Finally, perform the time-domain simulations of the coupled vessel-monopile system in irregular waves using the multi-body code SIMO and an external DLL that interacts with SIMO at each time step. The wave forces on the substructures in disturbed waves are calculated in DLL using the interpolation method described above. The total wave forces on the structure are returned to SIMO, and the motions of the coupled system are solved.

FLUID KINEMATICS IN SHORT-CRESTED WAVES

A short-crested sea is considered to be made up of component waves with different amplitudes, frequencies and directions. It can be characterized by a two-dimensional wave spectrum, which is often written as

$$S(\omega,\theta) = S(\omega)D(\omega,\theta) \tag{3}$$

$$\int_{-\pi}^{\pi} D(\omega,\theta)d\theta = 1 \tag{4}$$

It has been observed that the directional spreading function $D(\omega,\theta)$ is generally a function of both frequency and direction. However, for practical purposes, one usually adopts the approximation $D(\omega,\theta) = D(\theta)$; that is the frequency dependence of the directional function is neglected. One of the most widely used $D(\theta)$ is the cosine power function given by DNV (2010)

$$D(\theta) = \begin{cases} C(n)\cos^n(\theta-\theta_0) & |\theta-\theta_0| \le \pi/2 \\ 0 & |\theta-\theta_0| > \pi/2 \end{cases} \tag{5}$$

where θ_0 is the main wave direction about which the angular distribution is centered. The parameter n is a spreading index describing the degree of wave short crestedness, with $n\to\infty$ representing a long-crested wave field. $C(n)$ is a normalizing constant ensuring that Eqn. (4) is satisfied. It is found that

$$C(n) = \frac{1}{\sqrt{\pi}}\frac{\Gamma(1+n/2)}{\Gamma(1/2+n/2)} \tag{6}$$

Where Γ denotes the Gamma function. Consideration should be taken to reflect an accurate correlation between the actual sea state and the index n. Typical values for the spreading index for wind generated sea are n = 2 to 4. If used for swell, $n \ge 6$ is more appropriate (DNV, 2010). Because lifting operations are usually carried out in relatively low sea states, the spreading of the waves can be significant.

The spectra of the i^{th} component of kinematics (refers to fluid particle velocities or accelerations) in disturbed waves associated with a specified incident wave spectrum may be obtained in terms of the transfer functions $H_i(\omega, \theta)$ acquired from linear potential theory for different wave frequencies ω and directions θ. The required spectra are denoted by S_{ii} For long-crested wave, the spectra are related to the incident wave spectrum $S(\omega)$ in the main wave direction θ_0 as follows

$$S_{ii}(\omega,\theta_0) = \left|H_i(\omega,\theta_0)\right|^2 S(\omega) \tag{7}$$

For short-crested waves, the directional spreading function $D(\theta)$ should be taken into account, then

$$\begin{aligned} S_{ii}(\omega,\theta_0) &= \int_{\theta_1}^{\theta_2} \left|H_i(\omega,\theta)\right|^2 S(\omega,\theta)d\theta \\ &= \int_{\theta_1}^{\theta_2} \left|H_i(\omega,\theta)\right|^2 D(\theta)d\theta \cdot S(\omega) = \left|\bar{H}_i(\omega,\theta)\right|^2 S(\omega) \end{aligned} \tag{8}$$

To calculate the wave forces on the monopile in the disturbed wave field during lowering, the fluid kinematics $\ddot{\zeta}_s$ and $\dot{\zeta}_s$ in Eqn. (2) should be based on the disturbed fluid kinematics.

The fluid kinematics transfer functions in disturbed waves for unidirectional waves can be directly obtained from the panel method in the frequency domain, while the averaged transfer functions in short-crested waves can be calculated from Eqn (9). Thus, the realizations of the disturbed kinematics are generated. To compare the effects of the spreading on the responses of the monopile, the transfer functions of wave kinematics are first studied. The RAOs (the amplitude of the transfer function) of the kinematics in incident and disturbed waves considering long and short-crested waves with the same total energy are presented.

The RAOs of the wave elevation, fluid particle velocities in incident long-crested waves are compared with those in short-crested waves with different spreading indices, shown in Fig 2. The results at two regular wave frequencies are presented. The wave kinematics RAOs are symmetric about heading sea and beam sea directions. Compared to RAOs in long-crested waves, the RAOs of X-velocity reduce significantly in directions close to heading seas when implementing wave spreading index n = 2, while the RAOs close to beam seas increase. This is because the wave energy in the main wave direction reduces and the energy from the directions around the main direction contributes to the averaged RAOs. The same results can be observed for RAOs for Y-velocity. As the spreading indices increase, the wave energy is more concentrated to the main wave direction and the averaged RAOs in short-crested waves approach to those in long-crested waves. For wave elevation and particle velocity in Z direction, the RAOs in short-crested waves remain the same as those in long-crested waves since the wave spreading does not influence the quantities in the vertical direction.

When accounting for shielding effects from the vessel, the symmetry of the wave kinematics about the heading sea direction disappears. Fig. 3 to Fig. 5 provide the RAOs of wave elevation and fluid particle velocities in X and Y directions in disturbed waves with and without wave spreading, respectively. It is visible that the RAOs in disturbed waves are greatly affected by the vessel in short waves, while in long waves the RAOs are close to those in incident waves. This is due to the ability of the vessel diffraction decreases with increasing wave length. The RAOs in the leeward side of the vessel (from 0 *deg* to 180 *deg*) are significantly reduced in short waves when considering shielding

effects, while the RAOs in the windward side (from 180 *deg* to 360 *deg*) can be amplified, see $T = 7$ *sec* in Fig. 3 and $T = 5$ *sec* in Fig. 5.

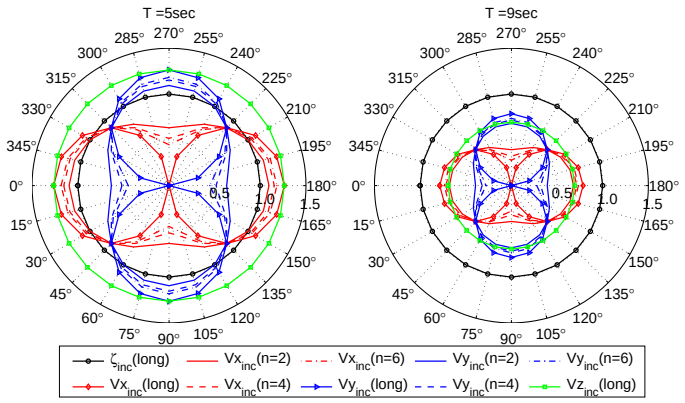

Figure 2: RAOs of fluid kinematics in incident long and short-crested ($n = 2, 4, 6$) waves ($x = -20$ *m*, $y = 30$ *m*, $z = 0$ *m*)

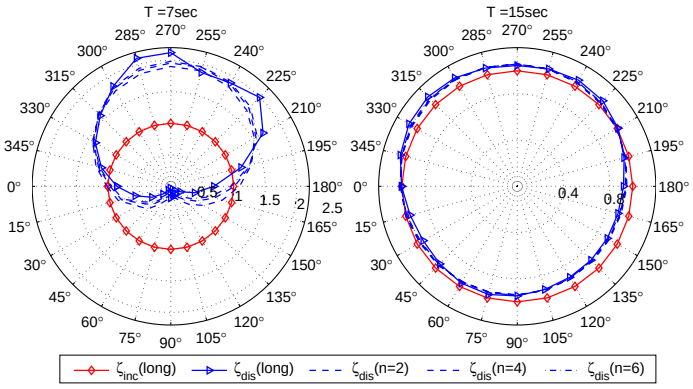

Figure 3: RAOs of wave elevations in disturbed long and short-crested waves ($n = 2, 4, 6$) waves ($x = -20$ *m*, $y = 30$ *m*, $z = 0$ *m*)

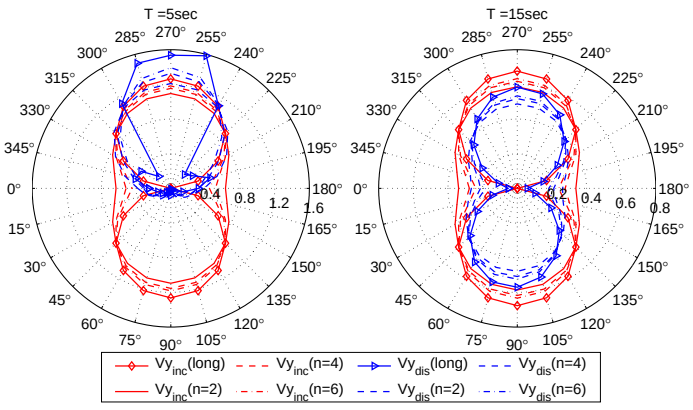

Figure 4: RAOs of Y-velocity in disturbed long and short-crested waves ($n = 2, 4, 6$) waves ($x = -20$ *m*, $y = 30$ *m*, $z = 0$ *m*)

When only unidirectional waves are considered, the differences between the RAOs in incident and disturbed waves are significant in short wave lengths. However, these differences are reduced considerably when including the effects from the spreading waves. For example, the averaged RAOs of X-velocity at $T = 5$ *sec* near 180 *deg* direction in disturbed waves are close to those in incident waves with spreading index $n = 2$ as shown in Fig. 5. This is because the spreading function averages the low RAOs in the leeward side and the large RAOs in the windward side of the vessel. Thus, it can be predicted that the shielding effects in short-crested waves would be less pronounced compared with the case when only long-crested waves are considered. Furthermore, similar to the results in incident waves, with increasing spreading index the disturbed RAOs in spreading waves are moving close to those in long-crested waves.

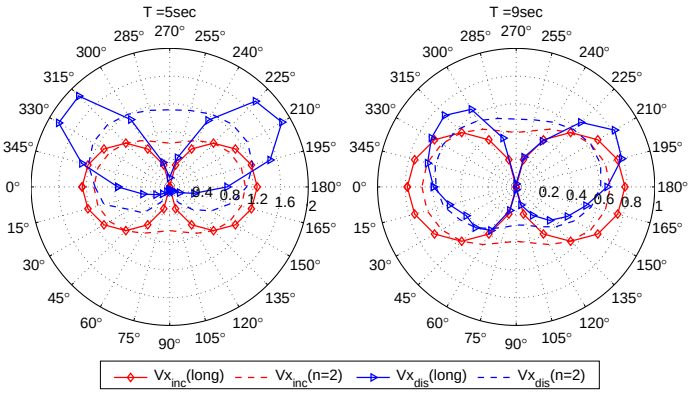

Figure 5: RAOs of fluid X-velocities in incident and disturbed waves with and without spreading ($x = -20$ *m*, $y = 30$ *m*, $z = 0$ *m*)

TIME-DOMAIN SIMULATIONS

Step-by-step integration methods were applied to calculate the responses of the lifting system using an iterative routine with a time step of 0.02 *sec*. The first order wave forces of the vessel were pre-generated using Fast Fourier Transformation (*FFT*) at the mean position. The fluid kinematics used to calculate the hydrodynamic forces on the monopile were calculated in the time domain using the interpolation of the pre-generated fluid kinematics at pre-defined wave points in disturbed waves.

The environmental condition of the time-domain simulations was chosen as $Hs = 2.0$ *m*. The wave spectral peak period *Tp* varied from 6 *sec* to 12 *sec*, thus covering a realistic range. At each combination of *Hs* and *Tp* the irregular waves were modelled by JONSWAP spectrum (DNV, 2010). In order to account for the variability of stochastic waves, 10 realizations of irregular waves were generated at each of the environmental conditions using different seeds. The duration of each realization was 20 *min*. Thus, the whole simulation corresponded to an operation with a duration of more than three hours.

RESULTS AND DISCUSSIONS

Responses in Long- and Short-crested Waves Without Shielding Effects

In the lifting operation of the monopile, the motions of the vessel affect the motions of the monopile through the lift wire and the gripper device, the motions of which in three directions are formulated in Eqn. (9):

$$\mathbf{s} = (\eta_1 + z\eta_5 - y\eta_6)\hat{i} + (\eta_2 - z\eta_4 + x\eta_6)\hat{j} + (\eta_3 + y\eta_4 - x\eta_5)\hat{k} \quad (9)$$

where η_1 to η_6 are the rigid body motions of the vessel and (x, y, z) is

the position of the crane tip or gripper relative to the fixed coordinates of the vessel body. Fig. 6 compares the standard deviations of crane tip motions (x = -20 m, y = 30 m, z = 80 m) in Z direction in incident waves with different spreading indices. The results are given with heading angles from 0 *deg* to 180 *deg*. The maximum Z-motions occur near beam sea due to the roll motions of the vessel. The motions increase with the wave peak period since the roll natural period of the vessel is close to 14 *sec*. Due to the spreading of the waves, it is clearly observed that the maximum crane tip motions close to beam sea are decreased and those close to heading and following seas are increased. The crane tip Z-motions in short-crested waves are larger than those in incident waves from 0 *deg* until near 60 *deg* with Tp = 8 *sec* and until near 45 *deg* with Tp = 12 *sec*. Thus, it is non-conservative to only apply long-crested waves at these directions if crane-tip Z-motions are critical to the whole lifting system using this vessel.

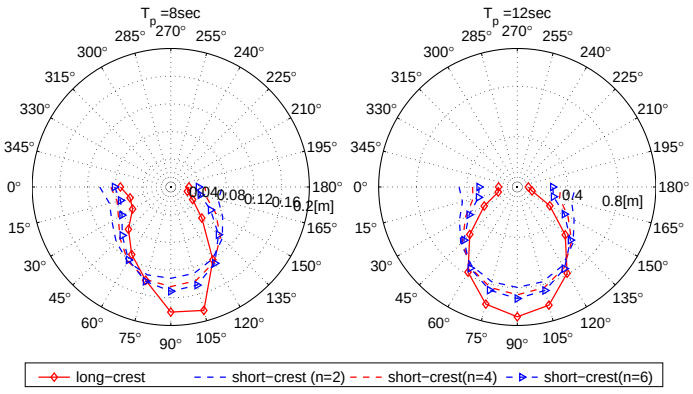

Figure 6: Crane-tip z-motions in incident waves with and without spreading (Hs = 2.0 m)

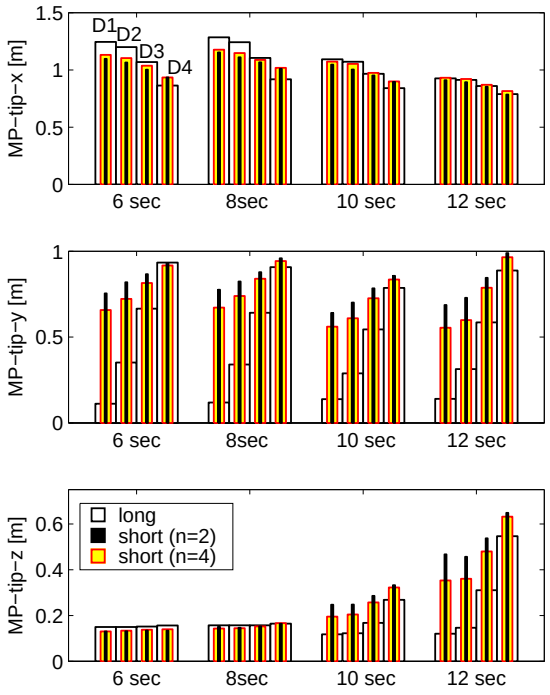

Figure 7: Standard deviation of MP tip motions in incident waves with and without spreading (H_s = 2:0m, for each T_p the directions from left to right are D_1 = 180 *deg*, D_2 = 165 *deg*, D_3 = 150 *deg*, D_4 = 135 *deg*)

The motions of the lower tip of the monopile during the lifting operation in incident waves are compared with different wave spreading conditions in Fig. 7. The results at four heading angles are provided. There are two contributions for the monopile motion: one is the direct wave excitation force on the MP and the other one is the induced motion from the vessel though the mechanical couplings. In short waves and near heading seas, the wave excitation force on the MP is dominant and the vessel motion is minor. Thus, the MP tip X-motion decreases at close to heading seas when considering wave spreading, while the tip Y-motion increase considerably. The roll motion of the vessel influences the lifting system in long waves, and the MP motions in Y and Z directions in short-crested waves are much higher those in long-crested waves at the directions considered, which are consistent with Fig. 6.

Responses in Long- and Short-crested Waves Considering Shielding Effects

Figures 8 and 9 compare the response time series (i.e., monopile tip displacements, lift wire tension and gripper device force) in disturbed long-crested and short-crested waves with spreading index n = 2. The response in short-crested waves are higher than those in long-crested waves when accounting for the shielding effects from the vessel. The reasons can be better explained by studying the response spectra. The spectra of the responses time series are plotted in Fig. 10. In order to compare the shielding effects, the response spectra in long-crested incident waves are also presented.

In short waves with Tp = 6 *sec*, the resonant motions of the monopile are excited, which corresponds to the peak frequency of the spectra at $\omega \approx 0.95$ *rad/s*. The hydrodynamic wave loads on the monopile dominate the response of the system in this case. In long waves, however, two peaks in the motion spectrum are observed. The peaks at $\omega \approx 0.95$ *rad/s* match the natural frequencies of the monopile rotational motion, while the peaks at $\omega \approx 0.45$ *rad/s* correspond to the vessel roll natural period. Due to the couplings of the monopile and the vessel, the increasing responses of the vessel in long wave dominate the motions of the system. The peak frequency of the wire tension and heave motion is consistently twice of the rotational peak frequency as one cycle of rotational motion induces two cycles of variations in the Z-motion and the wire tension.

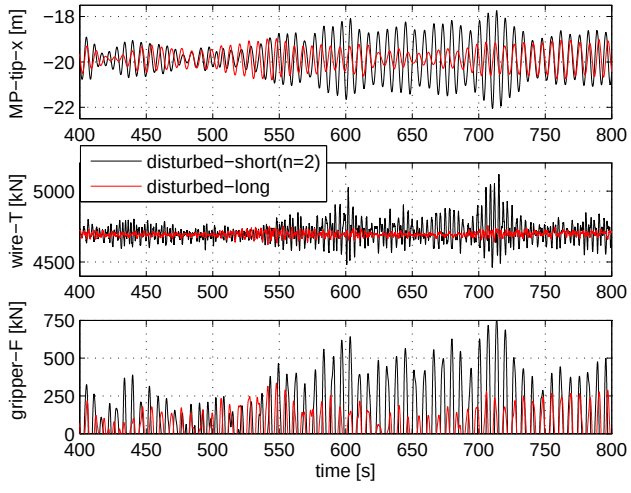

Figure 8: Time series of monopile responses in disturbed waves with and without spreading (Hs = 2.0 m, Tp=6 *sec*, Dir=150 *deg*)

For both wave conditions, the peaks at $\omega \approx 0.95$ *rad/s* in the response spectra, which correspond to the natural frequency of the rotational motions of the monopile, are significantly reduced when the shielding effects of the vessel are considered. In long waves with $Tp = 12$ *sec* the response peaks corresponding to the vessel motion do not decrease when considering shielding effects. These results indicate the significant influence of the shielding effects on the monopile motions, particularly in short waves when the wave frequencies are close to the natural frequencies of the monopile.

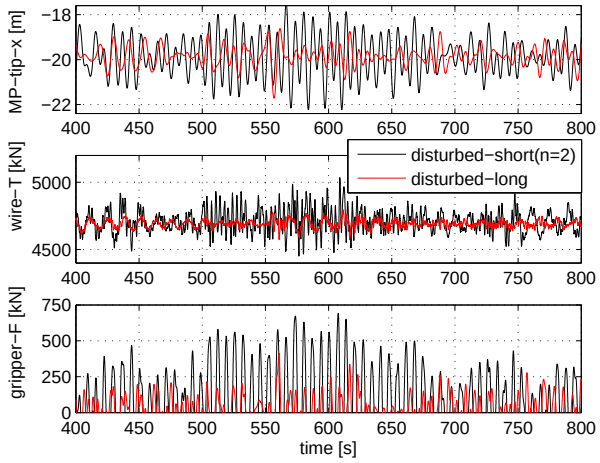

Figure 9: Time series of monopile responses in disturbed waves with and without spreading (*Hs*= 2.0 *m*, *Tp*=12 *sec*, *Dir*=150 *deg*)

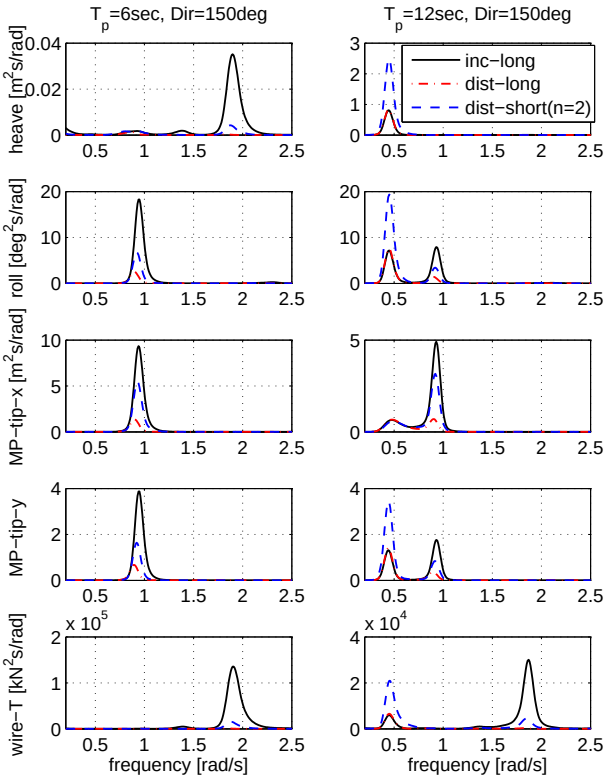

Figure 10: Response spectra in incident and disturbed waves with and without wave spreading (*Hs*= 2.0 *m*, *Dir*=150 *deg*)

By comparing the results in short and long-crested waves, it can be observed the reduction of spectra peaks at $\omega \approx 0.95$ *rad/s* in long-crested waves are more pronounced than those in short-crested waves when considering shielding effects. The reason is that the averaged wave kinematic RAOs in disturbed waves with spreading index $n = 2$ are higher than those in long-crested waves (see Fig. 3 to Fig. 5). Furthermore, the spreading of waves increases the peaks with $\omega \approx 0.45$ *rad/s*, which is consistent with Fig. 6 that the crane tip motion in short-crested waves are higher than those in long-crested waves with a heading angle of 150 *deg*.

The Influences of Wave Spreading on the Shielding Effects

Figures 11 and 12 compare the standard deviations of the monopile tip motions in incident waves with those in disturbed waves with long- and short-crested waves, respectively. For both cases, it can be seen the shielding effects reduce the responses significantly in short-waves and the reduction decreases with wave length. The shielding effects are more pronounced in long-crested waves than in short-crested waves. Thus, the reduction of extreme responses from shielding effects can be over-predicted if only considering long-crested waves.

Besides, the differences between responses at various headings in short-crested waves are much smaller than in long-crested waves. This is due to the spreading of the wave energy at neighbour directions, and the responses are averaged over directions. Moreover, from the results in disturbed waves at different wave periods and heading angles, it is possible to obtain the most suitable operational heading angle with minimum responses. In both long and short-crested cases, the most suitable angle is observed close to quartering seas in short waves and it moves towards to heading seas with increasing wave length. However, the responses at the most suitable heading angles in long-crested waves are always lower than those in short-crested waves. Thus, the wave spreading should be considered to avoid non-conservative results. The influences from the wave spreading are expected to reduce when using higher spreading index.

CONCLUSIONS

This study investigates the influences of the short-crested waves and the shielding effects from the floating installation vessel on the responses of the monopile lifting operation. The wave kinematics near the vessel were studied first in the frequency domain, followed by time-domain simulations. The shielding effects were included in the time-domain by interpolating fluid kinematics between predefined wave points near the floating vessel. The effects of the wave spreading on the responses in incident and disturbed waves were examined in detail. It is concluded that short-crested waves affect of the responses in both incident and disturbed waves significantly. The shielding effects can reduce the responses significantly, but the reduction are less in short-crested waves than in long-crested waves. Because the operational sea states are commonly short-crested, it is important to consider the effects from the directional waves to avoid non-conservative estimate of motions.

The averaged RAOs of the wave kinematics were obtained by applying the cosine spreading function and were compared with the RAOs in long-crested waves. The RAOs in incident long-crested waves can be greatly affected by the directional waves due to the spreading of the wave energy. The vessel shielding effects can result in a great decrease of the kinematics nearby and at the leeward side of the vessel, particularly in short wave lengths. However, the decrease is less considerably when accounting for the wave spreading.

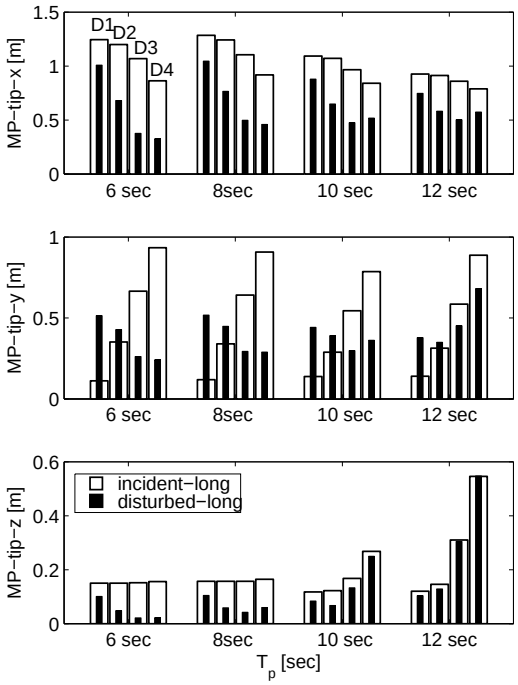

Figure 11: Standard deviation of MP tip motions in incident and disturbed waves in long-crested waves (H_s = 2:0m, for each T_p the directions from left to right are D_1 = 180 *deg*, D_2 = 165 *deg*, D_3 = 150 *deg*, D_4 = 135 *deg*)

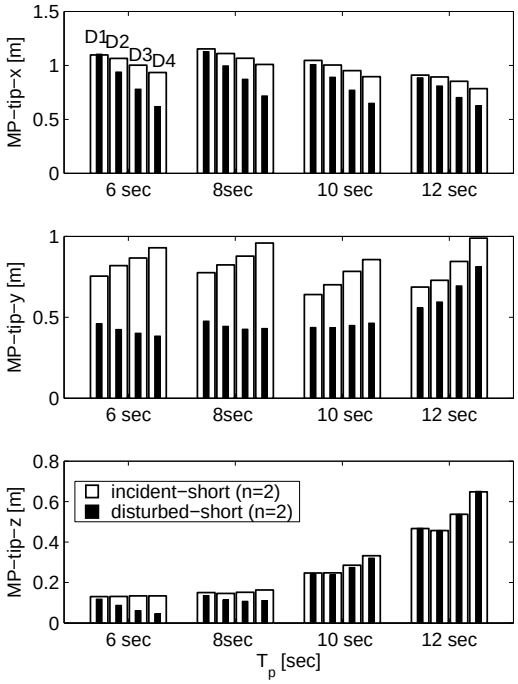

Figure 12: Standard deviation of MP tip motions in incident and disturbed waves with wave spreading (n = 2) (H_s = 2:0m, for each T_p the directions from left to right are D_1 = 180 *deg*, D_2 = 165 *deg*, D_3 = 150 *deg*, D_4 = 135 *deg*)

The shielding effects from the vessel bring pronounced reduction in the standard deviation of the monopile responses, in particular in short waves. Thus, it can be beneficial to utilize the effects to increase the operational weather window. The most suitable heading angle of the vessel are observed close to quartering seas in short waves and it moves towards to heading seas with increasing wave length. On the other hand, the responses considering shielding effects may be underestimated if only long-crested waves are applied. The spreading of wave energy narrows down the differences between the responses in incident and disturbed waves. This results in higher responses in short-crested waves than in long-crested waves at the most suitable heading angles. Therefore, short-crested waves are critical in predicting responses for the present scenario in both incident waves and disturbed waves with consideration of the shielding effects from the vessel.

ACKNOWLEDGEMENTS

The authors gratefully acknowledge the financial support from the Research Council of Norway granted through the Department of Marine Technology, Centre for Ships and Ocean Structures (CeSOS) and Centre for Autonomous Marine Operations and Systems (AMOS), NTNU. Thanks are extended to Erin Bachynski from MARINTEK for supporting the use of the software SIMO and Peter Sandvik from MARINTEK for valuable discussions.

REFERENCES

Baar, J., Pijfers, J., Santen, J., 1992. Hydromechanically coupled motions of a crane vessel and a transport barge. In: *24th Offshore Technology Conference*, Houston.

Bai, W., Hannan, M., Ang, K., 2014. Numerical simulation of fully nonlinear wave interaction with submerged structures: Fixed or subjected to constrained motion. *Journal of Fluids and Structures* 49, 534–553.

Battjes, J. A., 1982. Effects of short-crestedness on wave loads on long structures. *Applied Ocean Research* 4 (3), 165–172.

Chakrabarti, S. K., 1987. *Hydrodynamics of offshore structures*. WIT press.

DNV, 2008. *Wadam theory manual*. Det Norske Veritas.

DNV, October 2010. *Recommended Practice DNV-RP-C205, Environmental Conditions and Enviromental Loads*. Det Norske Veritas.

DNV, February 2014. *Recommended Practice DNV-RP-H103, Modelling and Analysis of Marine Operations.* Det Norske Veritas.

EWEA, 2014. *The European offshore wind industry - key trends and statistics 2013*. Report, The European Wind Energy Association.

Faltinsen, O., 1990. *Sea Loads on Ships and Ocean Structures*. Cambridge University Press.

Goda, Y., 2010. *Random seas and design of maritime structures*. World Scientific.

Inoue, Y., Islam, M. R., 2000. Numerical investigation of slowly varying drift forces of multiple floating bodies in short crested irregular waves. In: The *10th International Offshore and Polar Engineering Conference,* Seatlle, USA, May 28 - June 2.

Isaacson, M., Nwogu, O., 1987. Wave loads and motions of long structures in directional seas. *Journal of Offshore Mechanics and Arctic Engineering* 109 (2), 126–132.

Isaacson, M. d. S. Q., Sinha, S., 1986. Directional wave effects on large offshore structures. *Journal of Waterway, Port, Coastal, and Ocean Engineering* 112 (4), 482–497.

Kaiser, M. J., Snyder, B. F., 2013. Modeling offshore wind installation costs on the US outer continental shelf. *Renewable Energy* 50, 676–691.

Kumar, V. S., Deo, M., Anand, N., Chandramohan, P., 1999. Estimation of wave directional spreading in shallow water. *Ocean engineering* 26 (1), 83–98.

Lambrakos, K. F., 1982. Marine pipeline dynamic response to waves from directional wave spectra. *Ocean Engineering* 9 (4), 385–405.

Li, L., Gao, Z., Moan, T., Ormberg, H., 2014. Analysis of lifting operation of a monopile for an offshore wind turbine considering vessel shielding effects. *Marine Structures* 39, 287–314.

MARINTEK, 2012. SIMO - Theory Manual Version 4.0.

Marshall, P. W., 1976. Dynamic and fatigue analysis using directional spectra. In: *Offshore Technology Conference,* Houston, USA.

Mukerji, P., 1988. Hydrodynamic responses of derrick vessels in waves during heavy lift operation. In: *20th Offshore Technology Conference*, Houston, USA.

Nwogu, O., 1989. *Analysis of fixed and floating structures in random multi-directional waves*. PhD thesis, University of British Columbia.

Sannasiraj, S. A., Sundaravadivelu, R., Sundar, V., 2001. Diffraction radiation of multiple floating structures in directional waves. *Ocean engineering* 28 (2), 201–234.

Sun, L., Eatock Taylor, R., Choo, Y. S., 2012. Multi-body dynamic analysis of float-over installations. *Ocean Engineering* 51, 1–15.

Tao, L., Song, H., Chakrabarti, S., 2007. Scaled boundary FEM solution of short-crested wave diffraction by a vertical cylinder. *Computer methods in applied mechanics and engineering* 197 (1), 232–242.

Teigen, P. S., 1983. The response of a TLP in short-crested waves. In: *Offshore Technology Conference*, Houston, Texas, USA.

van den Boom, H., Dekker, J., Dallinga, R., 1990. Computer analysis of heavy lift operations. In: *22nd Offshore Technology Conference*, Houston, USA.

Zhu, S., Satravaha, P., 1995. Second-order wave diffraction forces on a vertical circular cylinder due to short-crested waves. *Ocean engineering* 22 (2), 135–189.